Therapeutic genome editing of triple-negative breast tumors using a noncationic and deformable nanolipogel

Peng Guo[a,b,c], Jiang Yang[a,b,c,1], Jing Huang[a,b,c], Debra T. Auguste[d,2,3], and Marsha A. Moses[a,b,c,2,3]

[a]Vascular Biology Program, Boston Children's Hospital, Boston, MA 02115; [b]Department of Surgery, Boston Children's Hospital, Boston, MA 02115; [c]Department of Surgery, Harvard Medical School, Boston, MA 02115; and [d]Department of Chemical Engineering, Northeastern University, Boston, MA 02115

Edited by Robert Langer, Massachusetts Institute of Technology, Cambridge, MA, and approved August 1, 2019 (received for review March 18, 2019)

Triple-negative breast cancer (TNBC), which has the highest mortality rate of all breast cancer, is in urgent need of a therapeutic that hinders the spread and growth of cancer cells. CRISPR genome editing holds the promise of a potential cure for many genetic diseases, including TNBC; however, its clinical translation is being challenged by the lack of safe and effective nonviral delivery systems for in vivo therapeutic genome editing. Here we report the synthesis and application of a noncationic, deformable, and tumor-targeted nanolipogel system (tNLG) for CRISPR genome editing in TNBC tumors. We have demonstrated that tNLGs mediate a potent CRISPR knockout of Lipocalin 2 (Lcn2), a known breast cancer oncogene, in human TNBC cells in vitro and in vivo. The loss of Lcn2 significantly inhibits the migration and the mesenchymal phenotype of human TNBC cells and subsequently attenuates TNBC aggressiveness. In an orthotopic TNBC model, we have shown that systemically administered tNLGs mediated >81% CRISPR knockout of Lcn2 in TNBC tumor tissues, resulting in significant tumor growth suppression (>77%). Our proof-of-principle results provide experimental evidence that tNLGs can be used as a safe, precise, and effective delivery approach for in vivo CRISPR genome editing in TNBC.

CRISPR genome editing | nanolipogel | triple-negative breast cancer | ICAM1

Triple-negative breast cancer (TNBC) is a breast cancer subtype characterized by the loss of estrogen receptor, progesterone receptor, and human epidermal growth factor receptor 2 (1). Over 32,000 patients are estimated to be diagnosed with TNBC in the United States in 2019, representing 12% of all new breast cancer cases (2). The incidence of TNBC is more frequent in young women of African origin and individuals carrying the hereditary breast cancer gene (BRCA) mutation (1, 3). Unfortunately, effective targeted therapies do not exist for TNBC patients, leaving surgery, chemotherapy, and radiotherapy as the only treatment options. The extremely aggressive and metastatic nature of TNBC, coupled with fewer treatment options, has resulted in the worst mortality rates among all breast cancer subtypes (1, 3), highlighting an urgent and unmet clinical need for novel precision medicines to treat TNBC.

CRISPR genome editing is a revolutionary biological tool to precisely engineer genes, and its clinical applications hold promise of a potential cure for many genetic diseases, including cancer (4, 5). To date, most studies of CRISPR genome editing therapy have focused on straightforward, monogenic diseases such as cystic fibrosis and hereditary tyrosinemia, and have achieved promising preclinical therapeutic benefits (5, 6). The therapeutic benefits of in vivo CRISPR genome editing on more complex, multigenic diseases (e.g., TNBC) are still unclear. Thus, we hypothesized that using targeted CRISPR genome editing therapeutics to precisely manipulate hereditary or somatic oncogenic mutations in TNBC tumors may bring a paradigm-shifting therapeutic approach for TNBC treatment. Until now, in vivo CRISPR genome editing has not been investigated as a targeted therapeutic for TNBC.

While in vivo CRISPR genome editing was recently demonstrated using cationic nanovectors (7–12), current cationic nanovectors suffer from several major drawbacks that significantly limit their clinical translation. Cationic nanovectors rely on cationic lipids or polymers to form electrostatic complexes with negatively charged CRISPR plasmids or guide RNAs, which ubiquitously destabilize cell plasma membranes and cause severe toxicity and intolerable adverse effects. Moreover, the genome editing systems delivered by these cationic nanovectors are endocytosed and subsequently trapped in cell endosomes and lysosomes, causing rapid degradation and insufficient transfection efficiency. In addition, most conventional CRISPR nanovectors lack disease-targeting functions and are passively taken up by the human mononuclear phagocytic system (MPS) during systemic circulation. These nonspecific nanovectors are difficult to adapt for treating diseases outside of the MPS, such as TNBC, in a precise and specific manner.

To overcome these obstacles, we report the development of a noncationic, deformable, and tumor-targeted nanolipogel system (tNLG) for tumor-specific CRISPR genome editing. In comparison

Significance

Triple-negative breast cancer (TNBC), which represents 12% of all breast cancers, is a devastating breast cancer subtype that occurs more frequently in women under 50 y of age, in African American women, and in individuals carrying a BRCA1 gene mutation. Because of the lack of therapeutic targets and limited treatment options, the prognosis for patients with TNBC remains the poorest of all patients with breast cancer. Here we report the synthesis and application of a novel CRISPR nanotherapeutic to effectively knock out Lipocalin 2 (Lcn2), a breast cancer-promoting gene, in TNBC tumors via in vivo genome editing, leading to a significant suppression of TNBC tumor growth. Our studies demonstrate that CRISPR genome editing is a promising targeted gene therapy approach for TNBC.

Author contributions: P.G., D.T.A., and M.A.M. designed research; P.G., J.Y., and J.H. performed research; P.G., J.Y., J.H., D.T.A., and M.A.M. analyzed data; and P.G., D.T.A., and M.A.M. wrote the paper.

Conflict of interest statement: P.G., J.Y., D.T.A., and M.A.M. are coinventors of a patent application filed by Boston Children's Hospital (US patent application no. 62/472,104; filed on 16 March 2017). J.H. is a consultant for Simcere Pharmaceutical Company. The other authors declare no other competing interests.

This article is a PNAS Direct Submission.

[1]Present address: Department of Comparative Pathobiology, College of Veterinary Medicine, Purdue University, West Lafayette, IN 47907.

[2]D.T.A. and M.A.M. contributed equally to this work.

[3]To whom correspondence may be addressed. Email: d.auguste@northeastern.edu or marsha.moses@childrens.harvard.edu.

This article contains supporting information online at www.pnas.org/lookup/suppl/doi:10.1073/pnas.1904697116/-/DCSupplemental.

Published online August 26, 2019.

with previously reported cationic CRISPR nanovectors, our engineered tNLGs feature 3 innovative advantages: 1) tNLGs employ a composition of zwitterionic and anionic lipids (termed "noncationic") and a deformable core–shell nanostructure that efficiently encapsulates CRISPR plasmids independent of electrostatic interaction, successfully eliminating cationic toxicity while maintaining high encapsulation efficiency (EE); 2) tNLGs utilize an antibody-guided strategy to selectively recognize and bind TNBC cells while sparing normal tissues, substantially improving the delivery of CRISPR plasmids in TNBC tumors; and 3) tNLGs feature a low particle elasticity that allows them to directly release CRISPR plasmids into the cytosol of targeted TNBC cells via a receptor-mediated membrane fusion pathway, effectively avoiding endosome entrapment within TNBC cells. In this proof-of-principle study, we explored the utility of tNLGs for the in vivo CRISPR knockout of Lcn2, an established breast cancer oncogene in an orthotopic TNBC model. Our results provide experimental evidence that in vivo CRISPR genome editing can halt TNBC tumor progression.

Results and Discussion

Design and Formulation of tNLGs. We have developed a tNLG to combinatorially deliver a pool of 3 CRISPR-Cas9 knockout plasmids for in vivo therapeutic genome editing of TNBC tumors. Our designed tNLG features a unique deformable core–shell nanostructure with a noncationic lipid bilayer and a biodegradable hydrogel core (Fig. 1*A*). The lipid bilayer comprises 2 lipids, zwitterionic 1,2-dioleoyl-sn-glycero-3-phosphocholine (DOPC) and anionic 1,2-distearoyl-sn-glycero-3-phosphoethanolamine-*N*-[carboxy(polyethylene glycol)-2000] (DSPE-PEG-COOH) (95/5, mol/mol), and alginate, a naturally occurring biopolymer approved by the US Food and Drug Administration for various biomedical applications (13, 14). These noncationic components ensure that tNLGs avoid cationic charge-induced toxicities. The 3 CRISPR plasmids were encapsulated in tNLGs and confined within the polysaccharide network of the alginate hydrogel and lipid bilayers. Each of the 3 CRISPR plasmids encodes a Cas9 nuclease and a 20-nt guide RNA sequence for identification and disruption of the Lcn2 gene in the genome of targeted human TNBC cells. Three CRISPR plasmids targeted to different DNA sequences of Lcn2 were used in combination to maximize the genome editing efficiency. ICAM1, a recently discovered TNBC nanotherapeutic target (15, 16), was utilized; the ICAM1 antibody was covalently conjugated on the surface of tNLGs at a density of ~3,000 antibodies per μm^2. Three other NLG formulations were also constructed as controls and tested together with commercially available cationic CRISPR transfection reagents (Ultracruz and Lipofectamine 2000) (Table 1).

Engineered tNLGs exhibited a uniform hydrodynamic diameter of ~110 nm with a polydispersity index (PDI) of less than 0.2, demonstrating its uniformity (Table 1 and Fig. 2*A*). The zeta-potential of the tNLG was slightly negatively charged. The deformable core–shell nanostructure of tNLGs was visualized by transmission electron microscopy (TEM) (Fig. 2*B*). Unlike the hollow bilayer structure of conventional liposomes, the presence of a dense and deformable hydrogel core in tNLGs was apparent. The elastic modulus of the tNLG structure was previously determined to be 1.3 MPa, using atomic force microcopy (16), significantly softer and more deformable than conventional solid lipid or polymer nanoparticles with elastic moduli ranging from 0.76 GPa to 1.2 GPa (17, 18). The EE of gene delivery via tNLGs was studied using 2 examples: scrambled CRISPR plasmid and scrambled small interfering RNA (siRNA). In Fig. 2*C*, the EEs of CRISPR plasmid in NLG formulations were determined to be 55 to 60%, significantly higher than conventional liposomes (neutral charge without hydrogel core, 27%) and at equivalent levels to 2 commercial cationic lipid-based transfection reagents (Lipofectamine 2000 and Ultracruz, 66 and 75%, respectively). A similar trend was observed in siRNA encapsulation, where tNLGs exhibited an EE as high as 80%. We attribute such high EE of tNLGs to its polysaccharide network of alginate confining the diffusion of biomacromolecules (e.g., DNA plasmids and siRNAs), resulting in retention within the lipid bilayer (19, 20). These results indicate that tNLGs are an efficient CRISPR delivery nanovector without reliance on the electrostatic interaction of cationic molecules.

We evaluated the storage stability of tNLG by incubating with 10% fetal bovine serum (FBS) supplemented cell cultured medium (DMEM). The dynamic light scattering (DLS) measurements

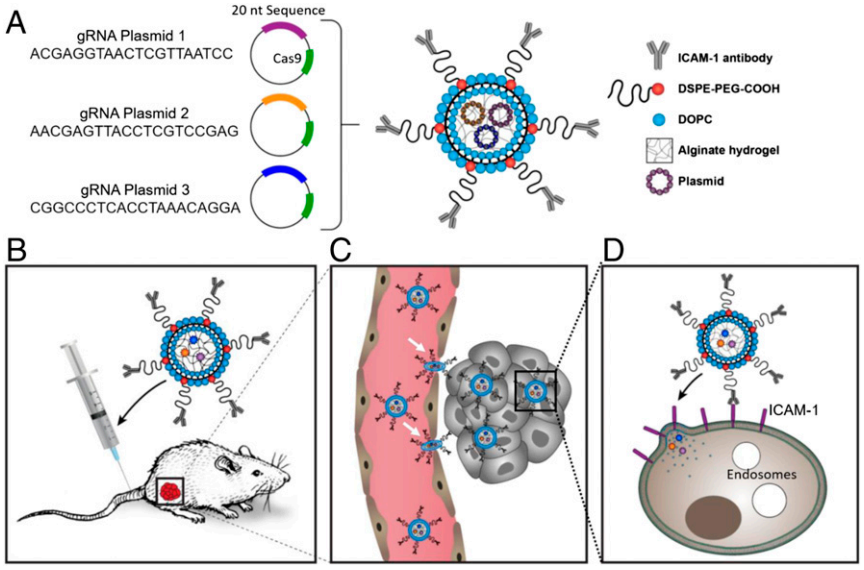

Fig. 1. Schematic illustration of tNLG structure and biomechanisms of in vivo CRISPR genome editing. (*A*) The design of tNLG for combinatorial delivery of 3 CRISPR plasmids. (*B*) The i.v. injection of tNLG for in vivo CRISPR genome editing of a TNBC tumor. (*C*) The deformable nanostructure of tNLG significantly improves its capability to cross leaky tumor endothelial barriers. Arrows highlight the events of transendothelial delivery of tNLGs. (*D*) CRISPR plasmids of tNLGs are directly released into the cytosol of targeted TNBC cells via ICAM1-mediated membrane fusion pathway.

Table 1. DLS characterization of tNLG and controls

Sample	Exterior	Interior	Payload	Size (nm)	PDI	Zeta-potential (mV)
Unmodified NLG	DOPC/DSPE-PEG	Alginate	CRISPR plasmid	104 ± 11	0.157	−6.2 ± 3.6
nNLG (nonspecific)	DOPC/DSPE-PEG-IgG	Alginate	CRISPR plasmid	112 ± 28	0.167	−4.6 ± 2.7
tNLG (tumor-specific)	DOPC/DSPE-PEG-aICAM1	Alginate	CRISPR plasmid	111 ± 23	0.102	−4.6 ± 3.8
tNLP (tumor-specific)	DOPC/DSPE-PEG-aICAM1	N/A	CRISPR plasmid	115 ± 35	0.154	−7.0 ± 6.1
UltraCruz	N/A		CRISPR plasmid	1,674 ± 210	0.216	−27.5 ± 10.6
Lipofectamine 2000	N/A		CRISPR plasmid	4,401 ± 3,726	0.447	−40.6 ± 9.9

showed that the hydrodynamic diameter of tNLGs remained unchanged in a 5-wk period (Fig. 2*D*) without forming precipitates, indicating that tNLGs are a highly stable CRISPR delivery system. Furthermore, due to the complete lack of cationic lipids, tNLGs are not expected to cause cytotoxicity. We confirmed this by evaluating the cytotoxicity of tNLGs in human TNBC MDA-MB-231 cells and 3 normal human cell lines (MCF10A, HEK293, and HUVEC; *SI Appendix*, Fig. S1). A commercial cationic CRISPR plasmid transfection reagent (Ultracruz) was used as a positive control. Fig. 2*E* and *SI Appendix*, Fig. S1 demonstrate that tNLGs

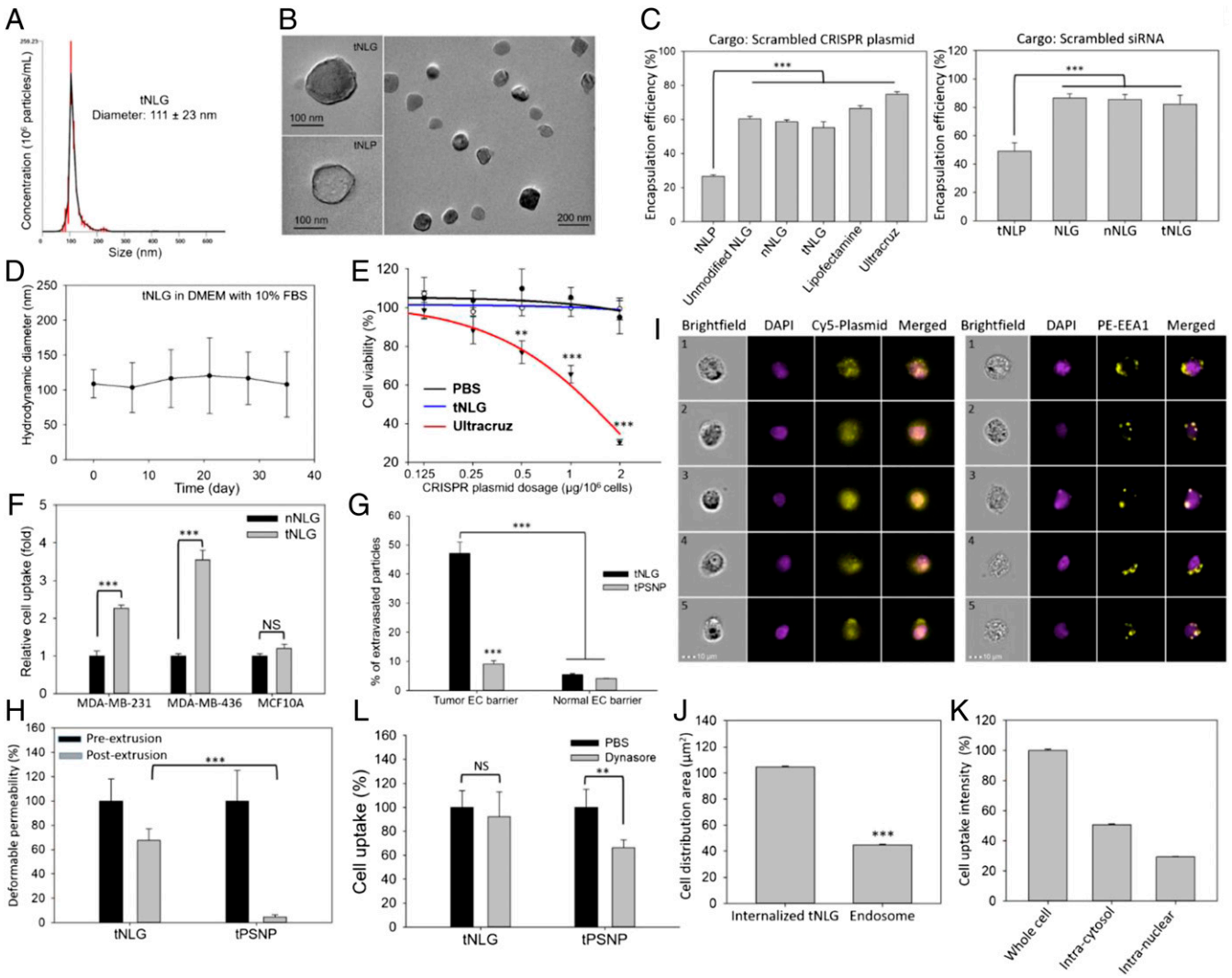

Fig. 2. Engineered tNLG as a CRISPR delivery nanovector. (*A*) Hydrodynamic diameter of tNLG. (*B*) The structures of tNLG (nanolipogel) and tNLP (nanoliposome without hydrogel core) were characterized by TEM. (*C*) Encapsulation efficiencies of tNLGs and controls for CRISPR plasmid and siRNA. (*D*) Storage stability of tNLG stored in DMEM with 10% FBS. (*E*) Cytotoxicity of tNLG and controls in MDA-MB-231 cells. (*F*) In vitro TNBC specificity of tNLG in comparison with nNLG. (*G*) Transendothelial capability of tNLG and tPSNP across the tumor endothelial cell (EC) barrier and the normal EC barrier. (*H*) Deformable permeability of tNLG and tPSNP across a 50-nm PCTE nanoporous membrane. (*I*) Representative fluorescent images showing intracellular locations of tNLG (Cy5), nucleus (DAPI), and endosomes (PE-EEA1) in MDA-MB-231 cells. (*J*) Quantified cell distribution area and (*K*) cell uptake of tNLG at whole cell, intracytosol, and intranuclear levels via imaging flow cytometry. (*L*) MDA-MB-231 cell uptake of tNLG and tPSNP under treatment of Dynasore, an endocytosis inhibitor. The significance was measured by 1-way ANOVA (in *C*) or 2-way ANOVA (in *E*) with Fisher post hoc test or unpaired Student's *t* test (*F*–*J*). NS, not significant; $^{**}P < 0.01$; $^{***}P < 0.001$.

displayed no obvious cytotoxicity in the tested range of plasmid dosage (0 μg to 2 μg per 10^6 cells), whereas Ultracruz exhibited severe cytotoxicity due to their highly positively charged composition. Moreover, in recent clinical trials, cationic gene delivery nanocarriers (e.g., polyethylenimine [PEI] or 1,2-dioleoyl-3-trimethylammonium-propane [DOTAP]-based nanoparticles) have been associated with severe adverse effects including fatigue, fever, and hypertension, regardless of systematic or local administration, which significantly impede their translation to the clinic (21).

TNBC-Targeted Delivery of CRISPR Plasmids by tNLGs. We determined the TNBC specificity of tNLGs using a cell uptake assay. We first fluorescently labeled ICAM1 antibody-conjugated tNLGs and IgG-conjugated nonspecific nanolipogels (nNLGs) by encapsulating Rhodamine-Dextran (MW 10 KDa) within the alginate core. We incubated these fluorescent tNLGs and nNLGs with 2 established human TNBC cell lines (MDA-MB-231 and MDA-MB-436) and nonneoplastic MCF10A cells. In Fig. 2*F*, ICAM1 antibody-directed tNLGs resulted in a 2- to 3-fold increase in cell uptake compared to nonspecific nNLG, positively correlating with the high ICAM1 overexpression on TNBC cell surfaces (15, 16). Nonneoplastic MCF10A cells lack ICAM1 expression, resulting in negligible tNLG uptake. These results indicate that tNLGs can selectively recognize and bind TNBC cells over normal breast cells, which may reduce their nonspecific toxicities in vivo, consistent with our previous findings using ICAM1 as a TNBC target (15).

Deformable tNLGs Breach in Vitro Tumor Endothelial Barrier via Its High Deformability. During in vivo CRISPR delivery, circulating tNLGs are required to efficiently breach the tumor endothelial barrier before reaching tumor cells. In this study, we measured the extravasation capability of our low elasticity (deformable) tNLG formulation using an established in vitro endothelial barrier assay (19, 22) in comparison with a high-elasticity control, a polystyrene nanoparticle with a similar diameter and ICAM1 antibody functionalization (tPSNP). As shown in Fig. 2*G*, we found that over 47% of tNLGs extravasated the tumor endothelial barrier, over 5-fold higher than the amount of tPSNPs. However, with a normal endothelial barrier, only 5.4% of tNLGs and 4.0% of tPSNPs extravasated, indicating that deformable tNLGs may selectively breach the tumor-associated endothelial barrier but not the normal endothelial barrier in vivo. We postulated that this extraordinary extravasation capability of tNLGs is due to its high deformability. To prove this hypothesis, we performed an established nanopore deformability assay (19, 23) by extruding both tNLG (~110 nm) and tPSNP (~110 nm) through a polycarbonate track-etched (PCTE) membrane with 50-nm nanopores. As shown in Fig. 2*H*, 67% of tNLGs successfully squeezed through the 50-nm nanopores, in comparison with merely 4% of stiff tPSNPs (postextrusion). This result demonstrates that deformable tNLGs can breach the tumor endothelial barrier more efficiently in vitro than their stiff counterpart which may, in turn, enhance its in vivo performance.

tNLGs Directly Release Payload into the Cytosol without Endosomal Entrapment. We reasoned that, after extravasation, deformable tNLGs selectively recognize and enter targeted TNBC cells via an ICAM1 receptor-mediated membrane fusion pathway, allowing tNLGs to directly release CRISPR plasmids into the cytosol of targeted TNBC cells without endosome entrapment. We validated this hypothesis by visualizing human TNBC cells transfected with tNLGs encapsulating fluorescent Cy5-labeled CRISPR plasmids using an imaging flow cytometry assay (24). MDA-MB-231 cell nuclei and endosomes were fluorescently labeled with DAPI and Phycoerythrin (PE)-conjugated early endosome antigen-1 (EEA1) antibodies, respectively. Representative fluorescent images (Fig. 2*I*) confirmed that CRISPR plasmids were delivered into the cytosol of TNBC cells by tNLGs. It is clear that most CRISPR plasmids were uniformly dispersed in the cytosol of MDA-MB-231 cells without being trapped in the endosomes. We analyzed 10,000 tNLG-transfected MDA-MB-231 cells to quantify their cell distribution area and cellular uptake of tNLGs at the whole-cell, intracytosol, and intranuclear levels using imaging flow cytometry. Importantly, we found that the cell distribution area of internalized tNLGs is 105 μm^2, ~2.3-fold larger than that of EEA1+ endosomes (45 μm^2; Fig. 2*J*), indicating that internalized CRISPR plasmids were not confined within endosomes. By colocalizing the cell nucleus with the distribution pattern of CRISPR plasmids inside TNBC cells, we confirmed that 29.3% of internalized CRISPR plasmids were successfully delivered into the nuclei of MDA-MB-231 cells by our engineered tNLG (Fig. 2*K*). This can be explained by the fact that, during the bioprocess of liposome/cell fusion, the artificial lipid bilayer of tNLGs directly fuses with the plasma membrane of targeted TNBC cells, without forming clathrin-coated pits (which later become endosomes). We have previously reported that this liposome/cell fusion pathway is strongly regulated by nanoparticle elasticity, independent of clathrin-mediated endocytosis (19). Therefore, we validated this membrane fusion-based intracellular delivery of tNLGs using a cell entry inhibition assay. We first pretreated MDA-MB-231 cells using 3 small molecules that inhibit clathrin-mediated endocytosis (Dynasore), caveolae-mediated endocytosis (Filipin), and macropinocytosis (Ethylisopropylamiloride), respectively. We then measured cell uptake of tNLGs in these inhibitor-treated cells and found that the cellular entry of tNLGs was not affected by any of these endocytosis inhibitors (Fig. 2*L* and *SI Appendix*, Fig. S2). In comparison, the cell entry of tPSNPs, fluorescein isothiocyanate (FITC)-labeled low density lipoprotein (FITC-LDL), and Rhodamine-Dextran (MW 70KD), which serve as positive controls for clathrin-mediated endocytosis, caveolae-mediated endocytosis, and macropinocytosis, respectively, was significantly impeded by inhibiting their cell entry pathways. These results indicate that the internalization of tNLGs predominantly depends on a membrane fusion pathway instead of endocytosis. This finding demonstrates an intracellular delivery advantage of tNLGs over conventional CRISPR delivery nanovectors with high elasticity; that is, tNLGs directly release CRISPR plasmids into the cytosol of targeted TNBC cells without endosomal entrapment.

In Vitro Gene Editing of TNBC Cells by tNLG. In order to demonstrate the therapeutic benefit of CRISPR genome editing, we selected Lcn2, an established oncogene that we have previously discovered to actively promote breast cancer progression and metastasis (25, 26), as the therapeutic target for our proof-of-principle TNBC-specific genome editing experiments in vitro and in vivo. We and others previously showed that Lcn2 levels are significantly up-regulated in tissues and urine samples from patients with invasive breast cancer (25, 27–30). We further confirmed that Lcn2 gene expression was significantly up-regulated in human TNBC cell lines (MDA-MB-231 and MDA-MB-436) in comparison with nonneoplastic MCF10A cells (Fig. 3*A*). The overexpression of Lcn2 in TNBC cells was also validated at the protein level, using immunofluorescent (IF) staining (Fig. 3*B*). In addition, to correlate Lcn2 expression with human TNBC clinical data, we analyzed the potential impact of Lcn2 gene expression on the overall survival of TNBC patients by querying the R2: Genomics Analysis and Visualization Platform database (https://hgserver1.amc.nl/, Datasheet: Tumor Breast Invasive Carcinoma-TCGA-1097). As observed in Fig. 3*C*, TNBC patients with high Lcn2 expression (cohort of 102 patients) demonstrated significantly worse prognosis than the low Lcn2 group (cohort of 76 patients, $P = 0.016$; log-rank test). We further analyzed the Lcn2 expression in different TNBC molecular subtypes using the same database (Fig. 3*D*) (Datasheet: Tumor breast (TNBC)-Brown-198). We found that elevated Lcn2 levels are more associated

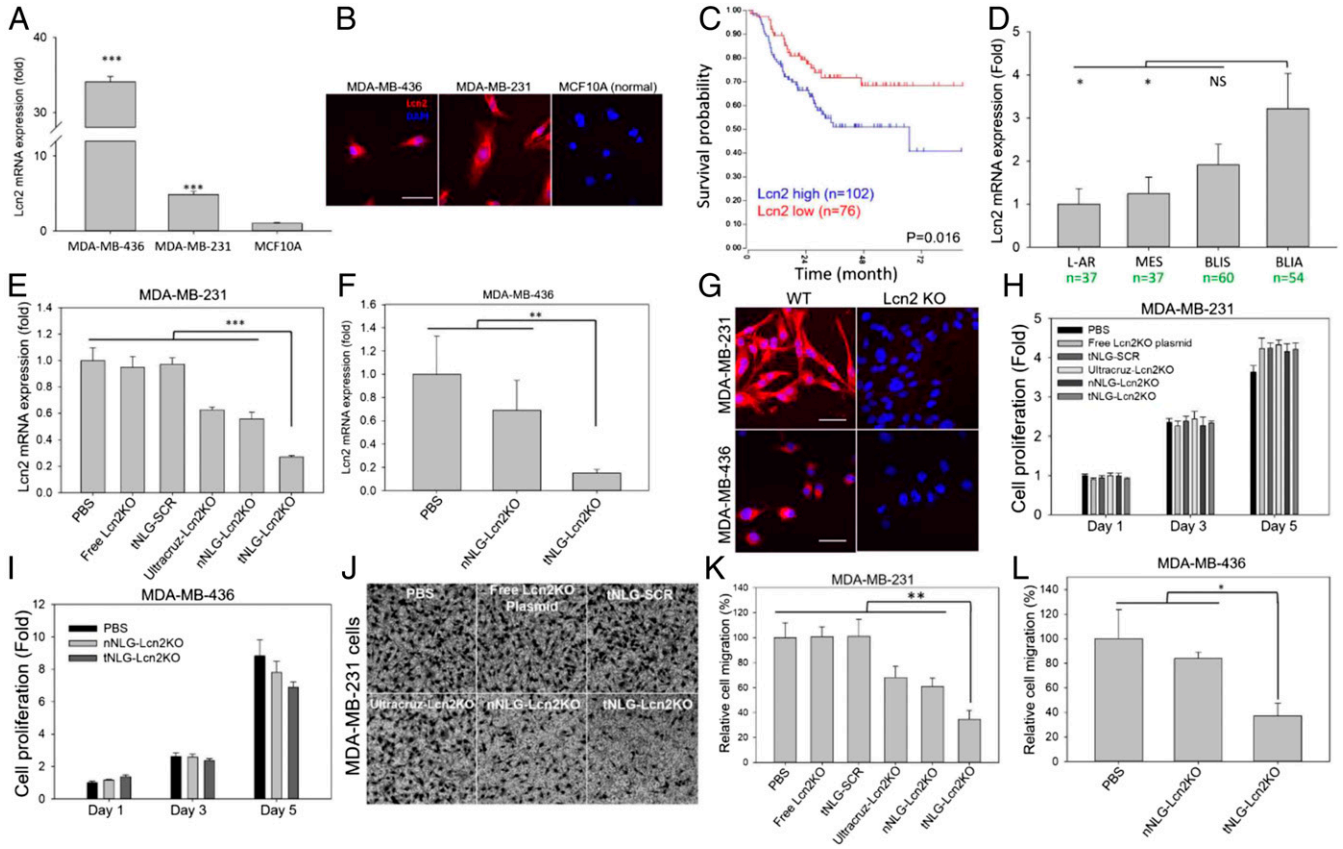

Fig. 3. Potent in vitro CRISPR genome editing by tNLG. Overexpression of Lcn2 in human TNBC cells was confirmed at both (*A*) gene expression by qRT-PCR and (*B*) protein expression by IF staining. (*C*) Correlation between overall survival and Lcn2 gene expression in 178 TNBC patients as shown with Kaplan–Meier analysis ($P = 0.016$, log-rank test). (*D*) Lcn2 gene expression in different molecular subtypes of TNBC: L-AR ($n = 37$), MES ($n = 37$), BLIS ($n = 60$), and BLIA ($n = 54$). In vitro genome editing efficiency was quantified by measuring CRISPR knockout of the Lcn2 gene at the transcription level in (*E*) MDA-MB-231 and (*F*) MDA-MB-436 cells by qRT-PCR. (*G*) Protein expression of Lcn2 in TNBC cells before and after Lcn2 CRISPR knockout was measured by IF staining. Cell proliferation of (*H*) MDA-MB-231 and (*I*) MDA-MB-436 with Lcn2 CRISPR knockout by tNLG and controls. (*J*) Representative images and (*K*) quantified cell migration of MDA-MB-231 cells with Lcn2 CRISPR knockout using a transwell migration assay. (Magnification: 100×.) (*L*) Quantified cell migration of MDA-MB-436 cells with the same Lcn2 CRISPR knockout by tNLG. (Scale bars: 20 μm.) The significance was measured by one-way ANOVA with Fisher post hoc test. $^*P < 0.05$; $^{**}P < 0.01$; $^{***}P < 0.001$.

with basal-like immunosuppressed (BLIS) and basal-like immunoactivated (BLIA), which represent 47 to 88% of all TNBCs together (31), than luminal androgen receptor (L-AR) and mesenchymal (MES) subtypes.

We next determined the in vitro genome editing efficiency of tNLGs by measuring the loss of Lcn2 expression using qRT-PCR. Fig. 3 *E* and *F* shows Lcn2 mRNA expression levels in TNBC cells treated with phosphate-buffered saline (PBS), free Lcn2 CRISPR knockout plasmid, tNLGs encapsulating scrambled CRISPR plasmid (tNLG-SCR, vehicle), a complex of Ultracruz and Lcn2 CRISPR knockout plasmid (Ultracruz-Lcn2KO), a nonspecific nNLG encapsulating Lcn2 CRISPR knockout plasmid (nNLG-Lcn2KO), and a TNBC-specific tNLG encapsulating Lcn2 CRISPR knockout plasmid (tNLG-Lcn2KO) at a dosage of 1 μg of plasmids per 10^6 cells. Among all treatment groups, tNLG-Lcn2KO exhibited the highest genome editing efficiency of ∼80% Lcn2 loss in both human TNBC cell lines (MDA-MB-231 and MDA-MB-436), significantly higher than the 30 to 50% Lcn2 loss after treatment with nonspecific nanovectors (nNLG-Lcn2 and Ultracruz). Free Lcn2 CRISPR knockout plasmid was incapable of mediating effective genome editing in the absence of intracellular delivery.

The potent Lcn2 CRISPR knockout by tNLG-Lcn2KO was also confirmed at the protein level in TNBC cells using IF staining (Fig. 3*G*). The tNLG-Lcn2KO transfected TNBC cells (MDA-MB-231 and MDA-MB-436) displayed a significant reduction of Lcn2 protein expression in accordance with the reduction in mRNA expression. These results indicated that tNLGs mediated potent and efficient CRISPR genome editing in human TNBC cells and significantly suppressed the expression of a specific oncogene target at both transcript and protein levels. Notably, the potent in vitro genome editing by tNLG-Lcn2KO does not require additional antibiotic selection as commercial cationic transfection reagents (e.g., Ultracruz).

Therapeutic Consequences of Lcn2 Loss in TNBC Cells. We determined the therapeutic functions of potent Lcn2 CRISPR knockout in TNBC cells by assessing malignant cell proliferation and migration. As shown in Fig. 3 *H* and *I*, Lcn2 CRISPR knockout in 2 TNBC cell lines did not alter their proliferation. However, the Lcn2 CRISPR knockout did potently impede cell migration in both MDA-MB-231 and MDA-MB-436 cells. The number of transmigrated TNBC cells in the tNLG-Lcn2KO group was reduced by over 60% in comparison with the PBS group (Fig. 3 *J–L*). We and others have previously reported that Lcn2 actively promotes breast tumor progression and metastasis by mediating the epithelial to mesenchymal transition (EMT) in breast cancer cells (25, 32, 33). Suppressing EMT has been demonstrated to inhibit tumor establishment and progression (34, 35). Therefore, we reasoned that Lcn2 CRISPR knockout in TNBC cells may be able to reverse EMT

and inhibit the mesenchymal phenotype of TNBC cells, subsequently attenuating TNBC migration and progression.

To evaluate the EMT phenotype changes caused by Lcn2 CRISPR knockout, we utilized a state-of-the-art quantitative phase imaging (QPI) method (36–38) to characterize and compare a panel of cell morphological and behavioral parameters between wild-type (WT, PBS group) and Lcn2 CRISPR knockout (Lcn2 KO, tNLG-Lcn2KO group) MDA-MB-231 cells. As shown in Fig. 4*A*, cell motion trajectories of WT and Lcn2 KO cells were recorded as time-lapse rose plots, where WT cells showed a more dispersed pattern than Lcn2 KO cells, due to the fact that WT cells had a significantly faster motility speed than Lcn2 KO cells, resulting in much longer migration distances (Fig. 4 *B* and *C*). We reasoned that the reduced migration capability of Lcn2 KO MDA-MB-231 cells was closely associated with their reversed EMT phenotypes. To verify this, we further analyzed the cell morphological parameters during cell movements, using the QPI approach. As shown in Fig. 4*D*, WT cells exhibited a classic mesenchymal cell phenotype with significantly longer filopodia during cell migration. In comparison, the Lcn2 KO cells significantly reduced their cell length by 40% and cell height by 10%, resulting in a significant inhibition of filopodia formation (Fig. 4 *E*–*H*). These results are in accordance with our and other reports that Lcn2 actively regulates EMT and alters breast cancer cell morphology (25, 32).

We further postulated that efficient Lcn2 CRISPR knockout may reverse EMT in TNBC cells and inhibit the mesenchymal phenotype associated with high mobility. To validate our hypothesis, we examined the expression of 2 EMT biomarkers (E-Cadherin and fibronectin) in both WT and Lcn2 KO TNBC cells. As shown in Fig. 4 *I* and *J*, we found that Lcn2 KO cells significantly reduced their fibronectin (mesenchymal biomarker) expression and increased the expression of E-Cadherin (epithelial biomarker). These results indicate that Lcn2 CRISPR knockout in TNBC cells significantly reduces aggressiveness by inhibiting EMT, at least partially, and may lead to a potent in vivo therapeutic benefit in TNBC therapy.

In Vivo Therapeutic Genome Editing in Orthotopic TNBC Tumors. We evaluated the tumor specificity and biodistribution of tNLG and nNLG in an orthotopic TNBC model using in vivo near-infrared (NIR) imaging (*SI Appendix*, Fig. S3). We labeled tNLG and nNLG with DiR, an NIR lipid dye, and i.v. injected fluorescently labeled tNLG-DiR or nNLG-DiR into orthotopic MDA-MB-231 tumor-bearing mice. At 24 h postinjection, we euthanized the animals and performed NIR imaging on excised TNBC tumors and major organs including liver, spleen, kidney, lung, heart, and brain (*SI Appendix*, Fig. S3 *A* and *C*). By quantifying the NIR signal of tumor (*SI Appendix*, Fig. S3*B*), we found that tumor uptake of tNLG-DiR represents 5% of total tNLG-DiR administered, which is 1.7-fold more than nNLG (nontargeting control, 3%). It is significantly higher than the average tumor accumulation of conventional nanomedicines (~0.7%) (39). This finding is consistent with our previously reported ICAM1 antibody-directed

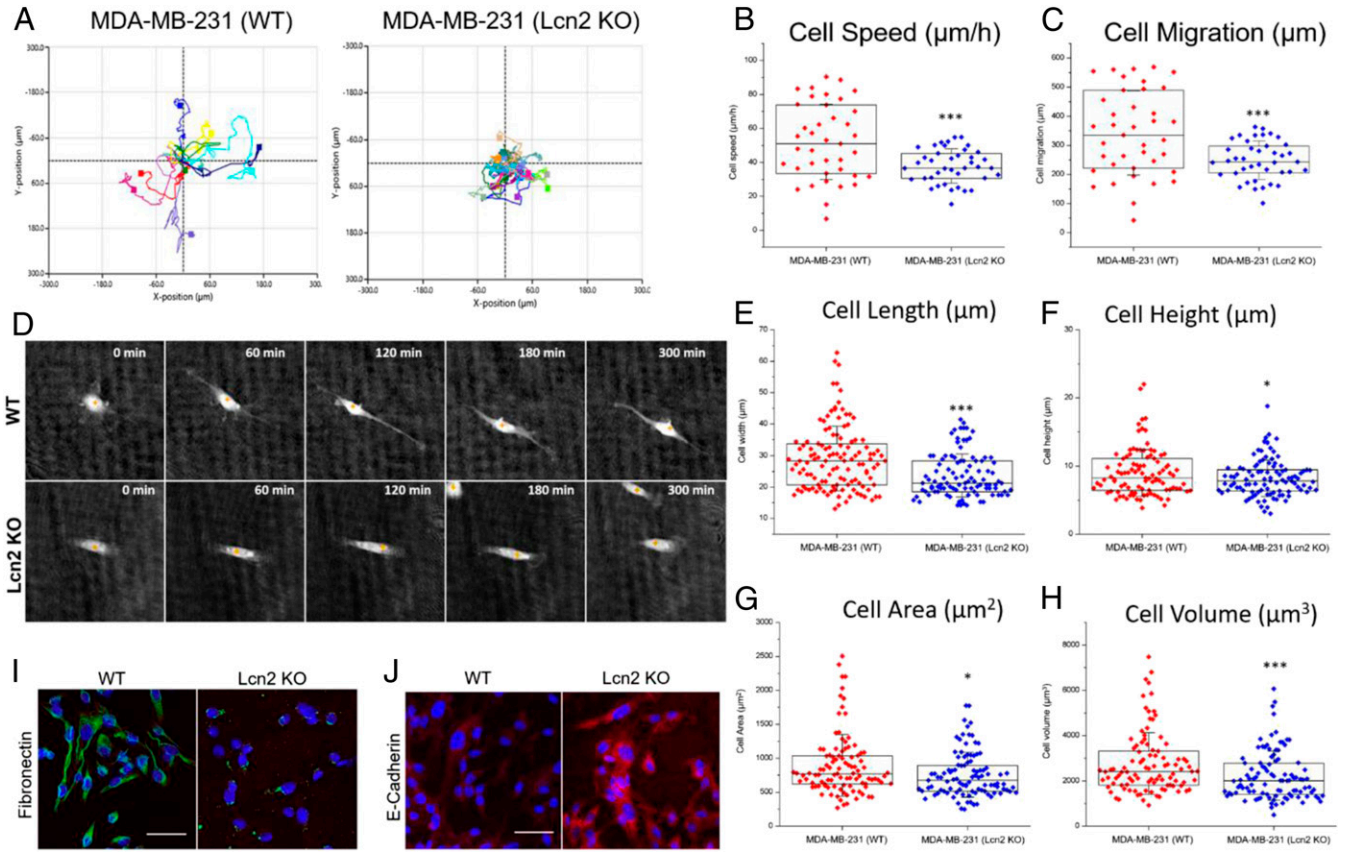

Fig. 4. CRISPR genome editing of Lcn2 inhibits EMT of TNBC cells. (*A*) Cell migration trajectories of WT and Lcn2 KO MDA-MB-231 cells. (*B*) Cell speed and (*C*) cell migration of WT and Lcn2 KO cells were quantified using QPI ($n \geq 45$ per group). (*D*) Representative images of WT and Lcn2 KO MDA-MB-231 cells in a cell migration event. (Magnification: 200×.) (*E*) Cell length, (*F*) cell height, (*G*) cell area, and (*H*) cell volume of WT and Lcn2 KO MDA-MB-231 cells were quantified using QPI ($n \geq 100$ per group). (*I* and *J*) Representative fluorescent images showing the protein expression of Fibronectin (green, mesenchymal marker) and E-Cadherin (red, epithelial marker) in WT and Lcn2 KO MDA-MB-231 cells. (Scale bars, 50 μm.) The significance was measured by unpaired Student's *t* test. $^{*}P < 0.05$; $^{***}P < 0.001$.

nanomedicines (15, 16, 40). Of the 6 organs analyzed (*SI Appendix*, Fig. S3*D*), liver and spleen are 2 major off-target sites for both tNLG-DiR and nNLG-DiR accumulation, accounting for 61% and 23 to 29%, respectively, of total administered nanomedicines. Notably, nonspecific nNLG-DiR tends to accumulate more in the spleen (29%) compared to tNLG-DiR (23%).

We determined the therapeutic efficacy of in vivo CRISPR genome editing using an orthotopic TNBC model (Fig. 5*A*). ICAM1 antibody-directed tNLG-Lcn2KO was weekly administered into MDA-MB-231 tumor-bearing mice via tail vein injection at an established dosage of 1 mg plasmid per kg (41). Other treatments including 1) PBS, 2) tNLG-SCR (vehicle), and 3) nNLG-Lcn2KO were tested as controls. All treatments were completed within 4 wk, and TNBC tumors were allowed to grow for another 4 wk without any treatment, in order to determine whether the therapeutic benefits of in vivo CRISPR genome editing can last after treatment termination. Correlating with previous biodistribution results, as shown in Fig. 5 *B* and *D*, tNLG-Lcn2KO exhibited a potent inhibitory effect on TNBC tumor growth compared with other control groups. Quantified tumor volume and mass analyses (Fig. 5 *B* and *C*) revealed that tNLG-Lcn2KO substantially attenuated TNBC tumor growth by 77% (in tumor volume) and 69% (in tumor weight), significantly more efficient than the nonspecific nNLG-Lcn2 group. Mouse body weights remained unchanged during treatment in all tested groups (Fig. 5*E*). We further quantified the in vivo CRISPR genome editing efficiency by measuring the loss of Lcn2 gene expression in TNBC tumors using qRT-PCR. As depicted in Fig. 5*F*, tNLG-Lcn2KO mediated a potent in vivo editing efficiency of ~81% in reference to PBS-treated tumors (sham group), significantly higher than that of the nonspecific nNLG-Lcn2KO group (53%). We also performed IF staining of Lcn2 and Ki67 in TNBC tumor tissues (*SI Appendix*, Fig. S4). We found that, after in vivo genome editing, Lcn2 protein levels significantly decreased in the tNLG-Lcn2KO treatment group compared with the sham group (*SI Appendix*, Fig. S4 *A* and *B*), closely correlating with their genome editing efficacy (Fig. 5*F*). Moreover, efficient Lcn2 knockout also significantly reduced Ki67-positive cell numbers in the tumors (*SI Appendix*, Fig. S4 *A* and *C*), indicating that tNLG-Lcn2KO inhibited TNBC cell proliferation in vivo and eventually led to tumor growth suppression. These in vivo results provide experimental evidence that efficient in vivo CRISPR genome editing by tNLGs can generate a potent and specific therapeutic benefit against TNBC tumor growth.

Lack of Off-Target Toxicity after In Vivo CRISPR Genome Editing. We evaluated the acute systemic toxicity of tNLG-Lcn2KO using an established blood chemistry assay (one dose, 1 mg of plasmid per

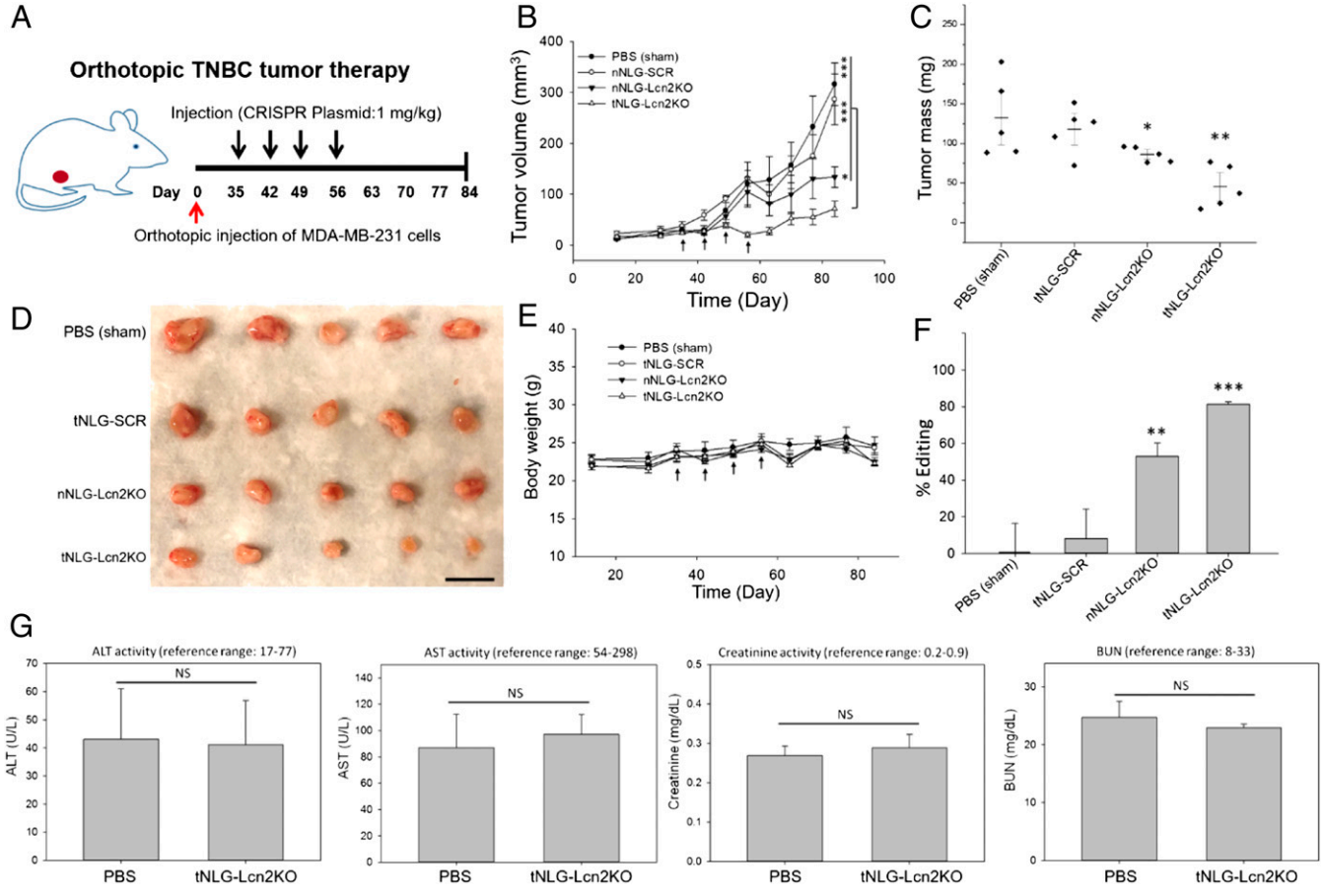

Fig. 5. In vivo CRISPR genome editing of Lcn2 potently attenuates TNBC tumor growth. (*A*) Schematic illustration of orthotopic TNBC therapy timeline. (*B*) Tumor progression was closely monitored by weekly tumor volume measurement. (*C*) Tumor mass at endpoint (day 84) was quantified in weight. (*D*) Images of excised TNBC tumors from mice treated with PBS (sham), tNLG-SCR, nNLG-Lcn2KO, or tNLG-Lcn2KO under a 28-d treatment regimen ($n = 5$ per group). (Scale bar: 1 cm.) (*E*) Mouse body weights were monitored weekly during different treatments. (*F*) In vivo genome editing efficiency of tNLG-Lcn2KO and other groups was determined by qRT-PCR. (*G*) Liver and renal toxicities of tNLG-Lcn2KO were determined in healthy mice by measuring serum levels of ALT, AST, Creatinine, and BUN. The significance was measured by 1-way ANOVA (in *C* and *F*) or 2-way ANOVA (in *B*) with Fisher post hoc test or unpaired Student's *t* test (in *G*). NS, not significant; $^*P < 0.05$; $^{**}P < 0.01$; $^{***}P < 0.001$.

kg per dose) (42). We i.v. injected tNLG-Lcn2KO into healthy nude mice at the same dosage for in vivo CRISPR genome editing therapy. At 48 h postinjection, we euthanized the mice and collected the serum from tNLG-Lcn2KO and PBS groups. In Fig. 5*G*, we measured the levels of aspartate aminotransferase (AST) and alanine aminotransferase (ALT), 2 liver toxicity biomarkers. We found that the AST and ALT levels of mice treated with tNLG-Lcn2KO were within normal ranges and exhibited no difference from those of mice treated with PBS, indicating no liver toxicity. We also evaluated the renal toxicity of tNLG-Lcn2KO by measuring creatinine and blood urea nitrogen (BUN) levels in the same mouse serum, and, similarly, no renal toxicity was observed for tNLG-Lcn2 treatment at the dosage of 1 mg of plasmid per kg. Because liver and spleen are 2 major off-target sites for tNLG-Lcn2KO accumulation, we performed hematoxylin and eosin staining on the liver and spleen of orthotopic TNBC tumor-bearing mice which received a full treatment of tNLG-Lcn2KO (4 doses, 1 mg of plasmid per kg per dose), in *SI Appendix*, Fig. S4. By comparing with other control groups, we did not observe any pathological changes in tNLG-Lcn2KO–treated liver and spleen. These in vivo results indicate that the nanoformulation of tNLG is relatively safe to use for in vivo CRISPR genome editing.

Conclusion

In summary, we report here the development of a noncationic, deformable, and TNBC-specific nanolipogel for in vivo CRISPR genome editing in human TNBC tumors. We have demonstrated that this tNLG mediated a potent in vivo editing efficacy of 81% in TNBC tumors, successfully suppressing the expression of Lcn2, a breast cancer oncogene, and attenuating 77% of TNBC tumor growth. The tNLGs represent a platform delivery system that can be used to target TNBC cells. For example, other established TNBC targets such as TROP2, EGFR, and EphA2 can also be used to guide tNLG to target TNBC tumors in vivo. Similarly, other TNBC oncogenes (e.g., PIK3CA, WNT, and Notch) can also serve as genome editing targets for Lcn2-negative TNBC subtypes (e.g., LAR and MES). This proof-of-principle study suggests that this tNLG formulation has a promising and broad potential for translating CRISPR genome editing into a novel precision medicine in cancer therapy.

Materials and Methods

See *SI Appendix, SI Materials and Methods* for details.

In Vitro CRISPR Genome Editing. The 3×10^5 cells were seeded in each well of a 6-well cell culture plate and incubated for 8 h at 37 °C with PBS, free Lcn2 CRISPR knockout plasmid, tNLG-SCR (vehicle), Ultracruz-Lcn2KO, nNLG-Lcn2KO, and tNLG-Lcn2KO at an equivalent plasmid concentration of 1 μg of plasmid per 10^6 cells. All cells were rinsed 3 times with PBS and further grown for 72 h. RNA was isolated using the Qiagen RNeasy Mini Kit according to the manufacturer's protocol. Complementary DNA was synthesized using the SuperScript Vilo Kit, and the levels of Lcn2 were quantified using StepOnePlus Real-Time PCR system (Applied Biosystems). All PCR samples were referenced to the expression of Glyceraldehyde 3-phosphate dehydrogenase.

In Vivo CRISPR Genome Editing. Mouse experiments were performed according to protocols approved by the Institutional Animal Care and Use Committees of Boston Children's Hospital. For tumor uptake and biodistribution studies, a total of 10^6 human TNBC MDA-MB-231 cells were orthotopically injected into the fourth mammary fat pad of female nude mice (Charles River). When tumors reached 200 mm^3 in volume, mice were randomized into 2 treatment groups ($n = 5$ for each group), which were i.v. injected with 1) nNLG-DiR, 2) tNLG-DiR (at dosage of 20 mg of lipids per kg of mouse weight). At 48 h postinjection, the mice were euthanized via CO_2, and the NIR fluorescence intensity of tumor and various excised organs (brain, heart, liver, lung, kidney, and spleen) was measured using an IVIS Lumina II system (Caliper).

For the in vivo genome editing studies, breast tumors were orthotopically implanted by injecting 10^6 MDA-MB-231 cells into the left fourth mammary fat pad of female nude mice (6 to 8 wk old). Tumors were allowed to develop for 5 wk until they became palpable, at which point mice were randomized into various treatment groups ($n = 5$ per group). Each group of mice was then treated with PBS (sham), tNLG-SCR, nNLG-Lcn2KO, and tNLG-Lcn2KO at an established plasmid dosage of 1 mg per kg per wk for 4 wk (41). All treatment injections were performed i.v. via tail vein injection in 50 μL of PBS. Tumor volume was monitored weekly by caliper. At week 8 after the initial treatment, all mice were euthanized by CO_2, and tumors were excised for analysis.

For the in vivo toxicity studies, PBS and tNLG-Lcn2KO were administered into healthy nude mice at a dose of 1 mg of CRISPR plasmid per kg via tail vein injection. At 48 h postinjection, mice were euthanized with CO_2 and 500 μL of whole blood was collected via cardiac puncture. Mouse blood was transferred to a BD Vacutainer and incubated for 20 min at room temperature to allow clotting. Serum was then collected after centrifuging at 2,000 × *g* for 10 min in a refrigerated centrifuge. Serum levels of ALT, AST, Creatinine, and BUN were determined using their activity assay kits purchased from Sigma-Aldrich with provided protocols.

Statistical Analysis. All of the experimental data were obtained in triplicate and are presented as mean ± SD unless otherwise mentioned. Statistical comparison by analysis of variance was performed at a significance level of $P < 0.05$ based on 1-way ANOVA or 2-way ANOVA or unpaired Student's *t* tests.

Data and Materials Availability. All data needed to evaluate the conclusions in the paper are present in the paper and/or *SI Appendix*.

ACKNOWLEDGMENTS. M.A.M. acknowledges the support of National Institutes of Health (NIH) R01CA185530 and the Breast Cancer Research Foundation. D.T.A. acknowledges the support of NIH 1DP2CA174495. We thank Kristin Johnson of the Vascular Biology Program at Boston Children's Hospital for assistance with the schematic illustrations.

1. W. D. Foulkes, I. E. Smith, J. S. Reis-Filho, Triple-negative breast cancer. *N. Engl. J. Med.* **363**, 1938–1948 (2010).
2. R. L. Siegel, K. D. Miller, A. Jemal, Cancer statistics, 2018. *CA Cancer J. Clin.* **68**, 7–30 (2018).
3. R. Dent *et al.*, Triple-negative breast cancer: Clinical features and patterns of recurrence. *Clin. Cancer Res.* **13**, 4429–4434 (2007).
4. P. D. Hsu, E. S. Lander, F. Zhang, Development and applications of CRISPR-Cas9 for genome engineering. *Cell* **157**, 1262–1278 (2014).
5. R. Barrangou, J. A. Doudna, Applications of CRISPR technologies in research and beyond. *Nat. Biotechnol.* **34**, 933–941 (2016).
6. H. Yin *et al.*, Therapeutic genome editing by combined viral and non-viral delivery of CRISPR system components in vivo. *Nat. Biotechnol.* **34**, 328–333 (2016).
7. H.-X. Wang *et al.*, Nonviral gene editing via CRISPR/Cas9 delivery by membrane-disruptive and endosomolytic helical polypeptide. *Proc. Natl. Acad. Sci. U.S.A.* **115**, 4903–4908 (2018).
8. J. A. Zuris *et al.*, Cationic lipid-mediated delivery of proteins enables efficient protein-based genome editing in vitro and in vivo. *Nat. Biotechnol.* **33**, 73–80 (2015).
9. H. Yin, K. J. Kauffman, D. G. Anderson, Delivery technologies for genome editing. *Nat. Rev. Drug Discov.* **16**, 387–399 (2017).
10. L. Li, S. Hu, X. Chen, Non-viral delivery systems for CRISPR/Cas9-based genome editing: Challenges and opportunities. *Biomaterials* **171**, 207–218 (2018).
11. R. S. Schuh *et al.*, In vivo genome editing of mucopolysaccharidosis I mice using the CRISPR/Cas9 system. *J. Control. Release* **288**, 23–33 (2018).
12. P. Wang *et al.*, Thermo-triggered release of CRISPR-Cas9 system by lipid-encapsulated gold nanoparticles for tumor therapy. *Angew. Chem. Int. Ed. Engl.* **57**, 1491–1496 (2018).
13. K. Y. Lee, D. J. Mooney, Alginate: Properties and biomedical applications. *Prog. Polym. Sci.* **37**, 106–126 (2012).
14. E. Caló, V. V. Khutoryanskiy, Biomedical applications of hydrogels: A review of patents and commercial products. *Eur. Polym. J.* **65**, 252–267 (2015).
15. P. Guo *et al.*, ICAM-1 as a molecular target for triple negative breast cancer. *Proc. Natl. Acad. Sci. U.S.A.* **111**, 14710–14715 (2014).
16. P. Guo *et al.*, Using atomic force microscopy to predict tumor specificity of ICAM1 antibody-directed nanomedicines. *Nano Lett.* **18**, 2254–2262 (2018).
17. J. Sun *et al.*, Tunable rigidity of (polymeric core)-(lipid shell) nanoparticles for regulated cellular uptake. *Adv. Mater.* **27**, 1402–1407 (2015).
18. L. Zhang *et al.*, Microfluidic synthesis of hybrid nanoparticles with controlled lipid layers: Understanding flexibility-regulated cell-nanoparticle interaction. *ACS Nano* **9**, 9912–9921 (2015).
19. P. Guo *et al.*, Nanoparticle elasticity directs tumor uptake. *Nat. Commun.* **9**, 130 (2018).
20. J. Park *et al.*, Combination delivery of TGF-β inhibitor and IL-2 by nanoscale liposomal polymeric gels enhances tumour immunotherapy. *Nat. Mater.* **11**, 895–905 (2012).

21. L. Liu *et al.*, Negative regulation of cationic nanoparticle-induced inflammatory toxicity through the increased production of prostaglandin E2 via mitochondrial DNA-activated Ly6C$^+$ monocytes. *Theranostics* **8**, 3138–3152 (2018).
22. A. Parodi *et al.*, Synthetic nanoparticles functionalized with biomimetic leukocyte membranes possess cell-like functions. *Nat. Nanotechnol.* **8**, 61–68 (2013).
23. F. R. Kersey, T. J. Merkel, J. L. Perry, M. E. Napier, J. M. DeSimone, Effect of aspect ratio and deformability on nanoparticle extravasation through nanopores. *Langmuir* **28**, 8773–8781 (2012).
24. S. Vranic *et al.*, Deciphering the mechanisms of cellular uptake of engineered nanoparticles by accurate evaluation of internalization using imaging flow cytometry. *Part. Fibre Toxicol.* **10**, 2 (2013).
25. J. Yang *et al.*, Lipocalin 2 promotes breast cancer progression. *Proc. Natl. Acad. Sci. U.S.A.* **106**, 3913–3918 (2009).
26. J. Yang, M. A. Moses, Lipocalin 2: A multifaceted modulator of human cancer. *Cell Cycle* **8**, 2347–2352 (2009).
27. M. Bauer *et al.*, Neutrophil gelatinase-associated lipocalin (NGAL) is a predictor of poor prognosis in human primary breast cancer. *Breast Cancer Res. Treat.* **108**, 389–397 (2008).
28. S. Candido *et al.*, Roles of neutrophil gelatinase-associated lipocalin (NGAL) in human cancer. *Oncotarget* **5**, 1576–1594 (2014).
29. B. Bauvois, S. A. Susin, Revisiting neutrophil gelatinase-associated lipocalin (NGAL) in cancer: Saint or sinner? *Cancers (Basel)* **10**, E336 (2018).
30. L. Roli, V. Pecoraro, T. Trenti, Can NGAL be employed as prognostic and diagnostic biomarker in human cancers? A systematic review of current evidence. *Int. J. Biol. Markers* **32**, e53–e61 (2017).
31. M. D. Burstein *et al.*, Comprehensive genomic analysis identifies novel subtypes and targets of triple-negative breast cancer. *Clin. Cancer Res.* **21**, 1688–1698 (2015).
32. G. Cheng *et al.*, HIC1 silencing in triple-negative breast cancer drives progression through misregulation of LCN2. *Cancer Res.* **74**, 862–872 (2014).
33. X. Leng, Y. Wu, R. B. Arlinghaus, Relationships of lipocalin 2 with breast tumorigenesis and metastasis. *J. Cell. Physiol.* **226**, 309–314 (2011).
34. M. A. Nieto, R. Y.-J. Huang, R. A. Jackson, J. P. Thiery, EMT: 2016. *Cell* **166**, 21–45 (2016).
35. J. Li *et al.*, Fisetin inhibited growth and metastasis of triple-negative breast cancer by reversing epithelial-to-mesenchymal transition via PTEN/Akt/GSK3β signal pathway. *Front. Pharmacol.* **9**, 772 (2018).
36. P. Guo, J. Huang, M. A. Moses, Characterization of dormant and active human cancer cells by quantitative phase imaging. *Cytometry A* **91**, 424–432 (2017).
37. J. Huang, P. Guo, M. A. Moses, A time-lapse, label-free, quantitative phase imaging study of dormant and active human cancer cells. *J. Vis. Exp.*, e57035 (2018).
38. P. Guo, J. Huang, M. A. Moses, Quantitative phase imaging characterization of tumor-associated blood vessel formation on a chip. *Proc. SPIE* **10503**, 105031O (2018).
39. S. Wilhelm *et al.*, Analysis of nanoparticle delivery to tumours. *Nat. Rev. Mater.* **1**, 16014 (2016).
40. P. Guo *et al.*, Dual complementary liposomes inhibit triple-negative breast tumor progression and metastasis. *Sci. Adv.* **5**, eaav5010 (2019).
41. J. D. Finn *et al.*, A single administration of CRISPR/Cas9 lipid nanoparticles achieves robust and persistent in vivo genome editing. *Cell Rep.* **22**, 2227–2235 (2018).
42. Q. Feng *et al.*, Uptake, distribution, clearance, and toxicity of iron oxide nanoparticles with different sizes and coatings. *Sci. Rep.* **8**, 2082 (2018).